ChemComm

COMMUNICATION

View Article Online
View Journal

Cite this: DOI: 10.1039/d0cc04187d

Received 16th June 2020,
Accepted 7th July 2020

DOI: 10.1039/d0cc04187d

rsc.li/chemcomm

Organoclay-derived lamellar silicon carbide/carbon composite as an ideal support for Pt nanoparticles: facile synthesis and toluene oxidation performance†

Runliang Zhu, *[abc] Qingze Chen, [abc] Jing Du,[abc] Qiuzhi He,[abc] Peng Liu,[d] Yunfei Xi [e] and Hongping He[abc]

A lamellar SiC/C composite was synthesized from organoclay *via* pyrolysis followed by salt-assisted magnesiothermic reduction. The *in situ*-formed carbon sheet within the restricted interlayer space of clay served as the carbon source and nanotemplate for forming SiC/C. With a large specific surface area, hierarchical porosity, available anchoring sites, good hydrophobicity, and thermal stability, SiC/C proved to be a promising support for Pt. The resulting Pt loaded SiC/C exhibited an excellent toluene oxidation performance.

Volatile organic compounds (VOCs) have aroused increasing concern because of their severe hazards to the environment and human health.[1–3] With low energy consumption and highly destructive efficiency, catalytic oxidation is regarded as an effective method for the abatement of VOCs.[4,5] Supported Pt catalysts are preferred for catalytic oxidation due to the high specific activity, especially for low-concentration VOCs among various catalysts.[1] Enormous efforts have been devoted to lowering the Pt loadings while maintaining a high catalytic performance of the catalyst.[6] Generally, the catalytic property of the supported Pt catalyst strongly depends on the structural characteristics of the support, which influences the distribution and size of Pt nanoparticles, the interaction between Pt and support, and the adsorption/diffusion of the reactants and products.[6] Traditional oxides (*e.g.*, Al_2O_3 and SiO_2) and zeolite are widely used to support Pt,[7,8] but the corresponding catalysts often suffer from serious deactivation in the presence of water vapor, due to the coverage of active sites by water molecules and the reaction between support and water at high temperature.[8,9] Porous carbon supports enable the supported Pt catalyst to possess both high activity and water-resisting ability,[10] but their inflammability limits their potential in practical applications. Moreover, additional treatments, such as oxidation and doping, are generally needed to increase the Pt anchoring sites on carbon materials.[11,12] Therefore, ideal supports with high stability, hydrophobicity, a large surface area, hierarchical porosity, and abundant anchoring sites for Pt are highly desirable for the high-performance supported Pt catalyst.

Silicon carbide (SiC) and its nanostructures have been used as a support to load metal nanoparticles for heterogeneous catalysis and fuel cells, owing to their excellent thermal/chemical stability, high thermal conductivity, and hydrophobic surface.[13,14] However, the limited surface area and porosity of SiC held back its applications in the abatement of VOCs. Recent studies indicated that a complex support could combine the advantages of different supports, thus enhancing the VOC oxidation performance of supported Pt catalysts, such as Pt/CeO_2-activated carbon[9] and Pt/graphene oxide–Fe_2O_3.[15] As such, one may expect that introducing carbon nanomaterials into nanostructured SiC would create an attractive SiC/C complex support with a large surface area, good porosity, and high hydrophobicity. However, the synthesis of SiC/C composite faces several difficulties: (1) the uniform mixing of nanostructured SiC and carbon nanomaterials is hard to achieve *via* simple mechanical blending; (2) the *in situ* formation of carbon nanomaterials (*via* chemical vapor deposition (CVD) and self-assembly)[16] on SiC involves a sophisticated process and delicate equipment; and (3) the synthesis of SiC nanoparticles (*e.g.*, *via* CVD and electrochemical etching) also depends on high cost and high energy consumption.[14]

Herein, we present a facile strategy for the synthesis of a lamellar SiC/C composite from organoclay *via* pyrolysis and subsequent salt-assisted magnesiothermic reduction (Fig. 1a),

[a] *CAS Key Laboratory of Mineralogy and Metallogeny, Guangdong Provincial Key Laboratory of Mineral Physics and Materials, Guangzhou Institute of Geochemistry, Chinese Academy of Sciences, Guangzhou 510640, China. E-mail: zhurl@gig.ac.cn*
[b] *University of Chinese Academy of Sciences, Beijing 100049, China*
[c] *Institutions of Earth Science, Chinese Academy of Sciences, Beijing 100029, China*
[d] *School of Environment and Energy, South China University of Technology, Guangzhou 510006, China*
[e] *School of Earth, Environmental and Biological Sciences, Queensland University of Technology (QUT), Brisbane, QLD, 4001, Australia*

† Electronic supplementary information (ESI) available: Experimental details; auxiliary analysis. See DOI: 10.1039/d0cc04187d

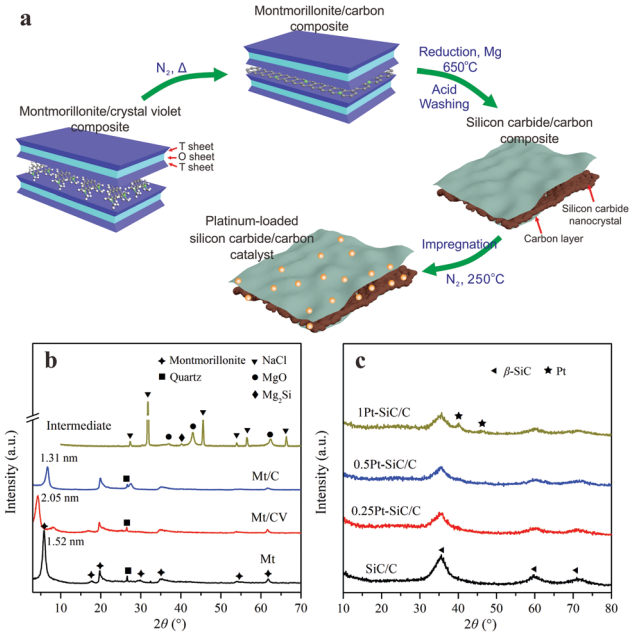

Fig. 1 (a) Schematic illustration of the synthesis of a lamellar SiC/C composite from organoclay. (b) XRD patterns of Mt, Mt/CV, Mt/C, and the intermediate after magnesiothermic reaction. (c) XRD patterns of the resulting SiC/C and the Pt-loaded SiC/C composites.

which could be scalably produced due to the cost-effective precursor and facile approach. The organoclay precursor was obtained by intercalating montmorillonite (Mt) with cationic crystal violet (CV, Fig. S1, ESI†), and acted as both silicon and carbon sources. The resulting SiC/C showed the characteristics of both SiC and C, *i.e.*, a large specific surface area (692 $m^2 g^{-1}$), hierarchical porosity (micro-, meso-, and macropores), thermal stability, and abundant anchoring sites (O- and N-containing functional groups). These structural merits of SiC/C enabled it as an attractive support for Pt nanoparticles (Fig. 1a). As a catalyst for toluene oxidation, the Pt-loaded SiC/C displayed high catalytic activity (with a complete conversion temperature of 185 °C), good cycling stability, and remarkable water resistance (with no deactivation at 190 °C under 5% water).

Mt is a 2 : 1 type clay mineral consisting of one octahedral (O) sheet sandwiched by two tetrahedral (T) sheets (Fig. 1a), giving a d_{001} value of 1.52 nm (Fig. 1b). The adsorption of cationic dye led to an evident increase in the basal spacing (2.05 nm), suggesting the multilayer or tilt arrangement of CV within the layer spaces.[17] Pyrolysis treatment converted Mt/CV to Mt/C with a significantly decreased basal spacing (1.31 nm), which gave an interlayer spacing of 0.35 nm (the thickness of one Mt layer being 0.96 nm). This value is close to the thickness of a single carbon layer, suggesting the generation of the graphene-like sheet within the restricted interlayer space of Mt.[17] The magnesiothermic reaction caused the formation of the intermediate, whose XRD pattern displayed the typical reflections of both MgO and Mg_2Si, besides NaCl. After eliminating the byproducts by acid washing, the target product SiC/C was obtained, which was confirmed by the distinct reflections of β-SiC (Fig. 1c) and the presence of amorphous carbon sheets (see TEM and XPS data below). Noticeably, Mg_2Si served as an important intermediate phase during the generation of SiC/C, probably *via* the reactions of SiO_2 (s) + 4Mg (l, g) → Mg_2Si (s) + 2MgO (s) and Mg_2Si (s) + SiO_2 (s) + 2C (s) → 2SiC (s) + 2MgO (s).[18] The sandwich structure (composed of a silicon-containing layer and carbon layer) of Mt/C facilitated the diffusion of the *in situ*-formed Mg_2Si to carbon, which was the key factor for the formation of SiC/C at the interface between silica and carbon.[19] In addition, NaCl as a heat scavenger could absorb the excess heat from the exothermic reaction and thus prevent the production of high-temperature phases (*e.g.*, spinel and α-SiC) (Fig. S2, ESI†). Finally, the as-prepared SiC/C was used as the support for Pt nanoparticles *via* a simple impregnation method. No reflections attributed to Pt were observed for 0.25Pt–SiC/C and 0.5Pt–SiC/C (Fig. 1c), probably due to the low loading amount and high dispersion of Pt nanoparticles. With the Pt loading amount increasing to 1%, the weak reflections of Pt emerged.

The SEM image of Mt/C showed a similar lamellar texture to raw Mt (Fig. 2a and b). The HRTEM image directly confirmed the sandwich structure consisting of an Mt layer and a carbon layer on Mt/C (Fig. S3, ESI†). Moreover, SiC/C possessed a porous and lamellar structure (Fig. 2c), somewhat retaining the morphology of Mt/C. The TEM images disclosed the overlapped or interconnected nanoparticles in the 2D structure of SiC/C (Fig. 2d and e), thus forming a hierarchically porous architecture (*i.e.*, mesopores in the lamellae and macropores built by the stacking of the layers). The interplanar spacing of 0.25 nm (assigned to the (111) plane of β-SiC) further verified the formation of SiC nanocrystals (Fig. 2f). Interestingly, we observed an approximately 1 nm-thick carbon layer wrapping around the SiC nanoparticles (Fig. 2f). The mass ratio of SiC and C was calculated to be ~4 : 1 according to the EDS data (Fig. S4, ESI†), corresponding to ~20 wt% C in the composite. This *in situ*-formed carbon sheet not only provided C element

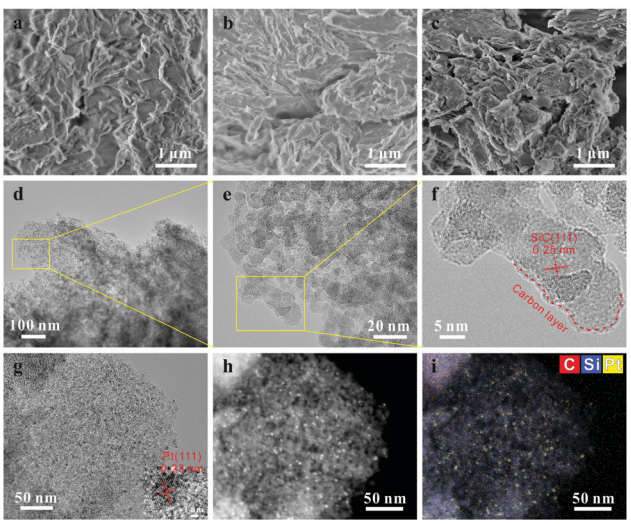

Fig. 2 SEM images of Mt (a), Mt/C (b), and SiC/C (c). TEM images (d and e) and HRTEM image showing the crystalline structure (f) of SiC/C. TEM images (g), dark-field TEM image (h), and EDS mapping (i) of 0.5Pt–SiC/C.

for the synthesis of SiC, but also acted as the nanotemplate for generating the lamellar SiC/C composite.

The TEM image of 0.5Pt–SiC/C indicated that Pt nanoparticles were well-dispersed with a relatively even size on the SiC/C support (Fig. 2g).[20] The good dispersion of Pt nanoparticles was further confirmed by the bright spots in the dark-field TEM image and the uniform distribution of C, Si, and Pt on 0.5Pt–SiC/C in the EDS mapping (Fig. 2h and i). With increasing Pt loadings, the size of Pt nanoparticles gradually increased (Fig. S5 and Table S1, ESI†). Moreover, SiC/C and 0.5Pt–SiC/C showed good N_2 adsorption capacities at all the relative pressures, suggesting the simultaneous presence of micro-, meso-, and macropores (Fig. S6a, ESI†). Compared with the calculated specific surface area (692 $m^2\ g^{-1}$) and pore volume (0.92 $cm^3\ g^{-1}$) of SiC/C, those of 0.5Pt–SiC/C slightly decreased (604 $m^2\ g^{-1}$ and 0.64 $cm^3\ g^{-1}$). The mesopore volume (in the range of 2–50 nm) of 0.5Pt–SiC/C diminished (Fig. S6b, ESI†), which implied the significant role of mesopore for the loading of Pt.[21]

The high-resolution Si 2p XPS spectrum of SiC/C could be fitted into a primary peak at 100.9 eV (Fig. 3a), assigned to Si–C of β-SiC.[22] The two minor peaks at 102.2 and 103.1 eV correspond to the small amount of Si bound to oxygen (*e.g.*, C_3Si-OH and C_2SiO_2).[22] Moreover, the high-resolution C 1s XPS spectrum was deconvoluted into two main components at 283.0 and 285.1 eV (Fig. 3b), which were attributed to C–Si and sp^2/sp^3 carbon, respectively.[22,23] These results further evidenced the presence of both SiC and carbon material on SiC/C. Several weak peaks at 286.2, 287.4, and 289.1 eV were attributed to C–O/C–N, C═O, and O–C═O, respectively.[23] Besides, the chemical states of N element (from CV) in SiC/C consisted of three components at 401.6, 400.4, and 398.3 eV (Fig. 3c), corresponding to graphitic, pyrrolic, and pyridinic N, respectively.[24] These O- and N-containing functional groups on the surface of SiC/C could enhance the interaction between metal and support, thus improving the dispersion and stability of metal nanoparticles.[1,11,25]

The high-resolution Pt 4f XPS spectra of the Pt-loaded SiC/C composites were compared (Fig. 3d). It was necessary to separate the Al 2p peak from the Pt 4f peak owing to the overlap of these two peaks in the range of 68–80 eV, since a very small amount of Al still remained in SiC/C even after acid washing several times (Fig. S4, ESI†). In our case, the Al 2p was set at ~74.1 eV, and the XPS spectra of Pt 4f could be fitted into two states, *i.e.*, Pt^0 species with the two binding energies of ~71.9 and ~75.3 eV, and Pt^{2+} species with a couple of peaks at ~73.8 and ~77.2 eV.[8,26] Generally, both the dissociative adsorption of oxygen from Pt^0 species and the extraction of lattice oxygen from PtO_x were involved in the catalytic oxidation over Pt-based catalysts, while the Pt^0 species were supposed to be more active for the catalytic process.[6,26] Based on the fitting results, the ratio of $Pt^0/(Pt^0 + Pt^{2+})$ decreased in the order 0.5Pt–SiC/C > 0.25Pt–SiC/C > 1Pt–SiC/C (Table S2, ESI†).

The H_2-TPR measurement of the Pt-loaded SiC/C catalysts exhibited two evident reduction peaks (Fig. 4a). The first peak at a low temperature (< 200 °C) was attributed to the reduction of PtO_x by H_2.[27] The surface oxygen adjacent to Pt species was also considered to contribute to the low-temperature peak.[28] The broad peak at 200–450 °C could be assigned to the reduction of surface oxygen distant from Pt[20] and oxygenated functional groups on the SiC/C surface.[29] Compared with 0.25Pt–SiC/C, 0.5Pt–SiC/C and 1Pt–SiC/C displayed a larger area of the low-temperature peak, which was associated with the greater loading amounts of Pt in the latter. Besides, 0.5Pt–SiC/C exhibited the lowest initial reduction temperature (94 °C) among the three catalysts, implying the most reducible characteristic.

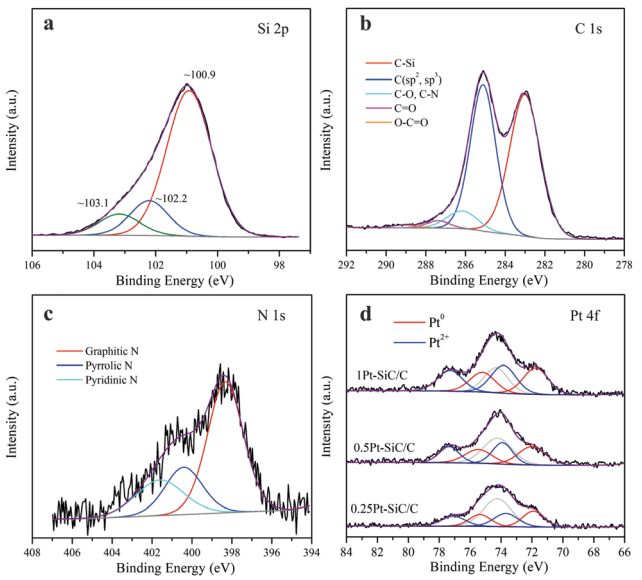

Fig. 3 High-resolution XPS spectra of Si 2p (a), C 1s (b), and N 1s (c) for SiC/C. High-resolution Pt 4f XPS spectra of the Pt-loaded SiC/C (d).

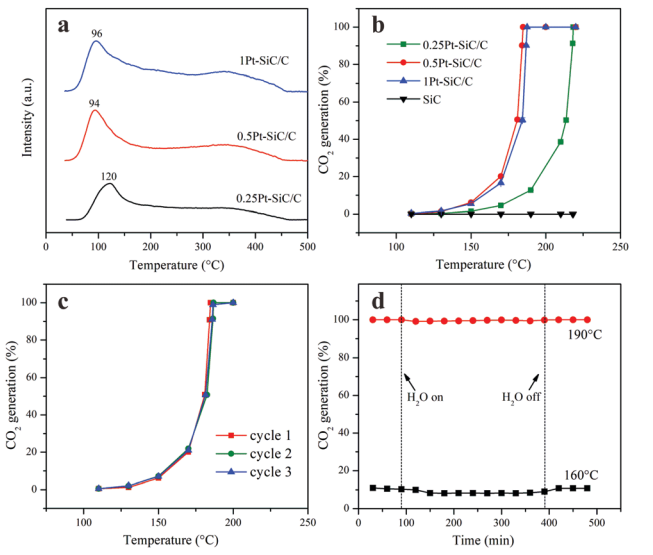

Fig. 4 (a) H_2-TPR profiles of the Pt-loaded Si/C composites; (b) CO_2 generation curves of toluene oxidation over SiC/C and various Pt-loaded SiC/C catalysts; (c) the catalytic oxidation for toluene over the 0.5Pt–SiC/C catalyst in three cycles; (d) effect of moisture (5% H_2O) on toluene oxidation over the 0.5Pt–SiC/C catalyst at 160 and 190 °C, respectively.

Pt-loaded SiC/C exhibited high activity for toluene oxidation, while no CO_2 generation was observed during the test temperature region for SiC/C without Pt (Fig. 4b). T90 (the temperature at 90% of CO_2 generation) of toluene over 0.5Pt–SiC/C was 184 °C, which was 3 and 34 °C lower than those over 1Pt–SiC/C (187 °C) and 0.25Pt–SiC/C (218 °C), respectively (Table S3, ESI†). 0.25Pt–SiC/C with high dispersion and small size of Pt nanoparticles showed a lower catalytic performance than 0.5Pt–SiC/C, mainly due to the smaller amount of Pt loading. In contrast, the inferior activity of 1Pt–SiC/C in comparison with 0.5Pt–SiC/C could be attributed to the low utilization of Pt atoms owing to the aggregation of Pt nanoparticles.[7] These results were quantitatively verified using the calculated TOF values (Table S3, ESI†). In addition, the high concentration of Pt^0 species was another important factor for the good catalytic activity of 0.5Pt–SiC/C.[21,30]

The stability test results showed no obvious change of CO_2 generation in three cycles (Fig. 4c), demonstrating that 0.5Pt–SiC/C had a superior catalytic stability for toluene oxidation. The good cycling durability should be attributed to the thermal stability of the SiC/C support[14] and limited carbon deposition on the surface due to a high catalytic activity of the supported Pt atoms.[6] The addition of 5% water vapor at 190 °C hardly decreased the CO_2 generation and 0.5Pt–SiC/C still maintained a complete conversion of toluene (Fig. 4d). The remarkable water-resisting property could result from the intrinsic hydrophobicity of SiC and C.[9,10] At 160 °C, the conversion of toluene to CO_2 slightly descended from 10% to 8%, but recovered to the original value when water vapor was cut off. These results indicated that moisture (5% water) did not have an evident inhibiting effect on the activity of the Pt-loaded SiC/C catalyst. In addition, as H_2O was also a byproduct of toluene oxidation, the good water-resisting property could enable the catalyst to adsorb O_2 more facilely,[31] consequently improving the catalytic activity. Without surface modification and complex designs, the obtained Pt-loaded SiC/C catalyst in our work possessed an outstanding catalytic performance from a practical point of view, in comparison with other supported Pt catalysts in the recently reported studies (Table S4, ESI†).

In summary, we successfully synthesized the lamellar SiC/C composite from organoclay *via* a facile synthesis strategy. SiC/C proved to be a promising support for Pt. The obtained Pt-loaded SiC/C exhibited an excellent catalytic oxidation performance of toluene. Our work offered a facile and cost-effective method for the synthesis of a novel lamellar SiC/C support from organoclay and provided an attractive supported Pt catalyst, which would have great potential in the practical abatement of VOCs.

This work was financially supported by the National Natural Science Foundation of China (41902040), the National Youth Top-notch Talent Support Program, the CAS Interdisciplinary Innovation Team (JCTD-2019-15), the Youth Innovation Promotion Association CAS (2020347), and the Guangdong Special Support Program (2017TX04Z243). The authors also thank H. Y. Fu from Tongji University for picture processing. This is contribution No. IS-2883 from GIGCAS.

Conflicts of interest

There are no conflicts to declare.

Notes and references

1 X. Hu, C. Li, Z. Sun, J. Song and S. Zheng, *Build. Environ.*, 2020, **168**, 106481.
2 Q. Chen, R. Zhu, L. Deng, L. Ma, Q. He, J. Du, H. Fu, J. Zhang and A. Wang, *Chem. Eng. J.*, 2019, **378**, 122131.
3 C. He, J. Cheng, X. Zhang, M. Douthwaite, S. Pattisson and Z. Hao, *Chem. Rev.*, 2019, **119**, 4471–4568.
4 P. Liu, G. Wei, H. He, X. Liang, H. Chen, Y. Xi and J. Zhu, *Appl. Surf. Sci.*, 2019, **464**, 287–293.
5 C. Wang, T. Chen, H. Liu, J. Xie, M. Li, Z. Han, Y. Zhao, H. He, X. Zou and S. L. Suib, *Appl. Clay Sci.*, 2019, **182**, 105289.
6 L. F. Liotta, *Appl. Catal., B*, 2010, **100**, 403–412.
7 R. Peng, S. Li, X. Sun, Q. Ren, L. Chen, M. Fu, J. Wu and D. Ye, *Appl. Catal., B*, 2018, **220**, 462–470.
8 C. Chen, Q. Wu, F. Chen, L. Zhang, S. Pan, C. Bian, X. Zheng, X. Meng and F.-S. Xiao, *J. Mater. Chem. A*, 2015, **3**, 5556–5562.
9 Z. Abdelouahab-Reddam, R. E. Mail, F. Coloma and A. Sepúlveda-Escribano, *Appl. Catal., A*, 2015, **494**, 87–94.
10 S. Morales-Torres, A. F. Pérez-Cadenas, F. Kapteijn, F. Carrasco-Marín, F. J. Maldonado-Hódar and J. A. Moulijn, *Appl. Catal., B*, 2009, **89**, 411–419.
11 M. Carmo, M. Linardi and J. G. R. Poco, *Appl. Catal., A*, 2009, **355**, 132–138.
12 G. Yang, Y. Li, R. K. Rana and J.-J. Zhu, *J. Mater. Chem. A*, 2013, **1**, 1754–1762.
13 R. Dhiman, E. Johnson, E. M. Skou, P. Morgen and S. M. Andersen, *J. Mater. Chem. A*, 2013, **1**, 6030–6036.
14 R. Wu, K. Zhou, C. Y. Yue, J. Wei and Y. Pan, *Prog. Mater. Sci.*, 2015, **72**, 1–60.
15 Z. Yan, Z. Xu, Z. Yang, L. Yue and L. Huang, *Appl. Surf. Sci.*, 2019, **467–468**, 277–285.
16 H. Fan and W. Shen, *ChemSusChem*, 2015, **8**, 2004–2027.
17 Q. Chen, R. Zhu, L. Ma, Q. Zhou, J. Zhu and H. He, *Appl. Clay Sci.*, 2017, **135**, 129–135.
18 X.-F. Zhang, Z. Chen, Y. Feng, J. Qiu and J. Yao, *ACS Sustainable Chem. Eng.*, 2018, **6**, 1068–1073.
19 J. Ahn, H. S. Kim, J. Pyo, J.-K. Lee and W. C. Yoo, *Chem. Mater.*, 2016, **28**, 1526–1536.
20 R. Peng, X. Sun, S. Li, L. Chen, M. Fu, J. Wu and D. Ye, *Chem. Eng. J.*, 2016, **306**, 1234–1246.
21 J. Zhang, C. Rao, H. Peng, C. Peng, L. Zhang, X. Xu, W. Liu, Z. Wang, N. Zhang and X. Wang, *Chem. Eng. J.*, 2018, **334**, 10–18.
22 S. Alekseev, E. Shamatulskaya, M. Volvach, S. Gryn, D. Korytko, I. Bezverkhyy, V. Iablokov and V. Lysenko, *Langmuir*, 2017, **33**, 13561–13571.
23 J. R. C. Salgado, R. G. Duarte, L. M. Ilharco, A. M. Botelho do Rego, A. M. Ferraria and M. G. S. Ferreira, *Appl. Catal., B*, 2011, **102**, 496–504.
24 Q. Chen, R. Zhu, Q. He, S. Liu, D. Wu, H. Fu, J. Du, J. Zhu and H. He, *Chem. Commun.*, 2019, **55**, 2644–2647.
25 A. Wong, Q. Liu, S. Griffin, A. Nicholls and J. R. Regalbuto, *Science*, 2017, **358**, 1427–1430.
26 X. Duan, Z. Qu, C. Dong and Y. Qin, *Appl. Surf. Sci.*, 2020, **503**, 144161.
27 H.-H. Liu, Y. Wang, A.-P. Jia, S.-Y. Wang, M.-F. Luo and J.-Q. Lu, *Appl. Surf. Sci.*, 2014, **314**, 725–734.
28 L. Nie, D. Mei, H. Xiong, B. Peng, Z. Ren, X. I. P. Hernandez, A. DeLaRiva, M. Wang, M. H. Engelhard, L. Kovarik, A. K. Datye and Y. Wang, *Science*, 2017, **358**, 1419.
29 J. Li, W. Tang, G. Liu, W. Li, Y. Deng, J. Yang and Y. Chen, *Catal. Today*, 2016, **278**, 203–208.
30 C. Chen, X. Wang, J. Zhang, C. Bian, S. Pan, F. Chen, X. Meng, X. Zheng, X. Gao and F.-S. Xiao, *Catal. Today*, 2015, **258**, 190–195.
31 B. Wang, B. Chen, Y. Sun, H. Xiao, X. Xu, M. Fu, J. Wu, L. Chen and D. Ye, *Appl. Catal., B*, 2018, **238**, 328–338.

